Int J Adv Manuf Technol (2017) 90:1383–1392
DOI 10.1007/s00170-016-9445-z

ORIGINAL ARTICLE

Study on laser cladding remanufacturing process with FeCrNiCu alloy powder for thin-wall impeller blade

Xu Lei[1] · **Cao Huajun**[1] · **Liu Hailong**[1] · **Zhang Yubo**[2]

Received: 17 June 2016 / Accepted: 4 September 2016 / Published online: 23 September 2016

Abstract The centrifugal compressor impeller is widely used in petroleum, chemicals, and other fields and is liable to failure in complicated working environment. Laser cladding as an advanced technology was used to remanufacture the failure impeller. And, remanufacture quality and service safety should be considered. In this paper, simulation and experiments were applied to study the remanufacturing process of failure thin-wall impeller blade. Firstly, a sequentially uncoupled 3D thermo-mechanical finite element (FE) model was developed to calculate temperature distribution and conduct mechanical analysis. Secondly, the impeller blade of repair region quality was studied based on microstructure analysis, microhardness, and tensile property tests. Finally, dynamic-balancing experiment, over-speed test, and dye penetration inspection were used to assess the security of remanufactured impeller. Numerical simulation showed that high temperature (about 1521 °C) and high residual stress (about 300 MPa) were distributed surrounding heat-affected zone (HAZ). And, experiments showed that the deformation of remanufactured impeller was 1.5 mm without no pores, cracks, slag inclusion, and other defects occurred in the remanufactured region.

Keywords Laser cladding · Failure impeller · Remanufacturing impeller · Finite element

✉ Cao Huajun
hjcao@cqu.edu.cn

[1] The State Key Laboratory of Mechanical Transmission, Chongqing University, Chongqing 400030, China

[2] National Key Laboratory for Remanufacturing, Academy of Armored Forces Engineering, Beijing 100072, China

1 Introduction

The centrifugal compressor impeller is widely used in petroleum, chemicals, military, and other important fields [1]. The impeller, the key component of turbo machines, often has failure due to complicated working environment (centrifugal force, unstable gas flow, etc.) [2, 3]. Failure impellers and blades not only cause significant economic losses to enterprises and society but also threaten people's lives [4]. With the development of technology, laser cladding technology is used extensively in the process of remanufacturing failure parts [5], which makes the remanufacture of failure impeller possible. As the remanufacture impeller has a very high demand for remanufacturing quality and safety, the laser cladding process and remanufacture quality should be studied.

Laser cladding technology is a surface modification technology, which can repair damaged parts. By adding cladding material onto the substrate surface and using high-energy density laser beam, the metallurgical bonding between the powder and thin layer on substrate surface was obtained. Laser cladding can significantly improve wear resistance, corrosion resistance, heat resistance, and other properties on the substrate surface with a little cost. In recent years, many studies and researches focus on the remanufacturing of failure components. In order to reduce the cracks generating in the cast iron cylinder heads, Dong et al. [6] investigated the remanufacturing technique of cylinder heads with laser cladding. And, no cracks existed in the interior or surface of build-up cladding according to the test. Hu et al. [7] used laser cladding technology to repair GH864 alloy rotating blades of flue gas turbines, and the failure reasons were analyzed. The formation of cracks in single crystal (SX) turbine blades is a common problem for aero-engines. Rottwinkel et al. [8] used multi-layer cladding to replace single crystal material to repair the cracks of turbine blades. And, repair quality met the

Fig. 1 Failure open impeller

turbine blades requirements. Process parameters are crucial to the quality of laser cladding. Lin [9] employed the Taguchi method to determine the optimal parameters for tenon repair on a steam turbine blade using multi-layer laser cladding. The results showed the repaired tenon met minimum design standards with regard to tensile strength. Jiang et al. [10] and Chew et al. [11] conducted simulation and experiment research to residual stress produced in the process of laser cladding restoration. The above researches have promoted the development of laser cladding in remanufacture field.

As the blade of centrifugal compressor impeller has a thin wall, the thickness of a common impeller is 1~6 mm, which limits the optimization of laser cladding scanning-path [11] during the impeller restoration and easily causes subsidence and excessive fusion with inappropriate laser cladding parameters. Meanwhile, the complex surface blade inclined assembly on the impeller shaft; traditional fixture is no longer suitable for impeller remanufacture [12]. The clamping system should be improved. Impeller is a high-speed rotation part and centrifugal force caused by high-speed rotation is even up to 500 MPa [13]. In order to avoid safety accident, higher requirements on strength and quality of remanufactured impeller were proposed than that of other remanufacturing components. So, a kind of proper laser cladding powder with remanufacturing process should also be studied. According to the above researches and taking the above factors into consideration, there are seldom studies and researches about the remanufacturing on failure thin-wall impeller blade with complex surface.

In this paper, for fracture failure impeller, the remanufacturing of failure thin-wall impeller blade with complex surface in laser cladding was studied. Firstly, based on the requirements of laser cladding powders, FeCrNiCu alloy powder with good mechanical and thermal properties was adopted. Secondly, temperature distribution of laser cladding, residual stress and strain, and deformation were analyzed in the experiment and finite element simulation. Then, the impeller blade of repair region quality was studied by the microstructure analysis, microhardness, and tensile property test. Finally, the remanufactured impeller safety was assessed by dynamic-balancing experiment, over-speed test, and dye penetration inspection.

2 Remanufacturing process with FeCrNiCu alloy powder analysis

2.1 Laser cladding process

Laser cladding is an advanced surface modification technology which can repair damaged parts. By adding cladding material onto substrate surface, wear resistance, corrosion resistance, heat resistance, and other properties can be improved. There are several factors affecting the laser cladding quality, for instance, alloy powders, parameters, operational knowledge, and environment. Among these factors, the laser cladding alloy powders and process parameters are the most important. The process parameters of laser cladding include laser power, laser spot diameter, defocus parameters, powder-feed rate, scanning speed, and preheating temperature. These parameters have great influence with very complicated process on dilution rate, crack, surface roughness, and density of cladding parts. When selecting powder, several factors also should be considered. (1) The cladding powder should have a good formability and a good wettability with the substrate. (2) The mechanical properties and physical properties of powder are similar to the substrate, which can satisfy the work condition of the impeller. (3) The chemical composition and thermal physical properties of powder are similar to that of the substrate.

In this paper, the parameters of laser cladding and alloy powder were obtained after multiple sets of experiments. The parameters and alloy powder have reference values to the remanufacturing of impeller and other components.

Table 1 Mechanical properties of FV520B

Yield stress (MPa)	Tensile strength (MPa)	Young's modulus (GPa)	Density (kg/m^3)	Vickers hardness (HV)	Poisson's ratio
1029	1170	210	7860	380	0.3

Table 2 Chemical composition of FeCrNiCu and FV520B (wt.%)

	Cr	Ni	Cu	C	Si	Mn	Nb	Fe
FV520B	13.0–14.5	5.0–6.0	1.3–1.8	≤0.07	≤0.07	≤1.00	0.25–0.45	Bal.
FeCrNiCu	14.05–15.10	4.21–4.53	4.41~4.45	0.07~0.12	1.20~1.51	0.60~0.72	0.12–0.22	Bal.

2.2 Experimental process with FeCrNiCu alloy powder

Due to the centrifugal compressor has very complicated working conditions, corrosion, wear, and other failure modes are happened. In this paper, the failure impeller with some materials lost in blades was studied, as shown in Fig. 1. The failure open impeller has 18 blades including 9 long blades and 9 short blades, and the diameter is 240 mm. The rated speed is 28,696 r/min. The material is FV520B precipitation-hardening martensitic stainless steel [14]. Due to its high strength, good ductility, great corrosion resistance, and excellent welding performance, FV520B has been widely used in impeller manufacturing. The mechanical properties and chemical composition are shown in Tables 1 and 2 [15]. In this paper, FeCrNiCu alloy powder was adopted to remanufacture the impeller and the chemical composition is shown in Table 2.

A fiber laser with a power 4 kW, which can realize the coaxial powder-feed, was used. The particle size of the powder was −140~+320 mesh. Laser power was set at 1.1 kW, laser scanning speed was 5 mm/s, powder-feed rate was 8.0 g/min, laser spot diameter was 3 mm and carrier flow was 150 L/h. The nitrogen (N_2) was used to protect the laser cladding pool during the laser cladding and a six-axis robot was used to control the laser cladding path as shown in Fig. 2. In order to improve the remanufactured impeller quality, an experiment with same parameters was carried out on thin plate (FV520B) to test the remanufacturing quality. After finishing the laser cladding, the specimens were polished with standard metallographic procedures. Then, the corresponding metallurgical microstructure at specimens' cross section was checked by optical microscopy. The microhardness of cladding coatings was obtained by microhardness tester.

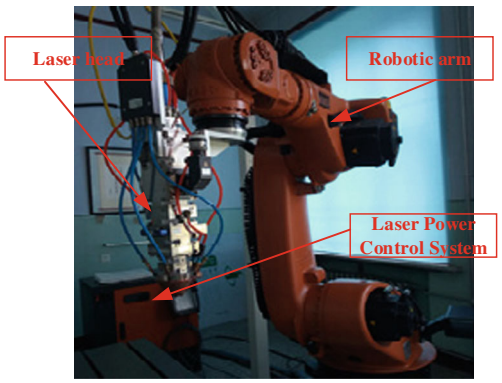

Fig. 2 Robot control system

3 Thermo-mechanical FE modeling

A sequentially uncoupled 3D thermo-mechanical FE model was developed to calculate the temperature distribution first, and then, the thermal results were applied to the mechanical analysis [18]. And, the residual stress was obtained by ANSYS software. All the computational procedures can be summarized in a flow chart in Fig. 3.

3.1 Temperature field analysis in laser cladding

Understanding the temperature field in laser cladding process could be of great importance to the study outcomes of cladding process including thermally induced cracking and stress, and phase transformation occurred in heat-affected zone (HAZ). In thermal analysis, the laser cladding process was simulated by applying heat flux to the elements. In finite element method (FEM), the element "birth and death" technology was used. Initially, all the repair region's elements were removed and killed. Once the laser cladding started, the "death elements" were activated segment by segment, and heated elements cooled down until the next cycle. The temperature history files of nodes were stored for the next residual stress calculation. The material properties relevant to thermal analysis are density, specific heat capacity, latent heat capacity, and solidus/liquidus

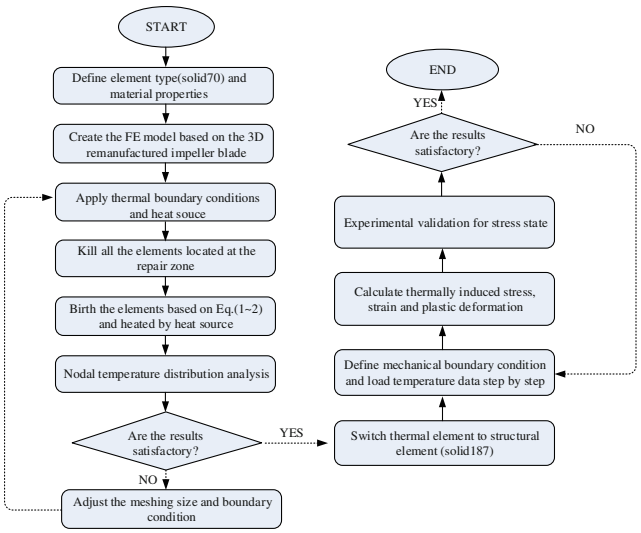

Fig. 3 Laser cladding numerical procedure flowchart

Table 3 Temperature-dependent thermal, physical, and mechanical properties of FeCrNiCu and FV520B

FeCrNiCu/FV520B	25 °C	300 °C	400 °C	600 °C	950 °C	1050 °C	1300 °C
Elastic modulus E/GPa	206/196	175/181	168/164	160/152	148/147	130/142	122/134
Yield strength σ_s/MPa	1076/1097	978/985	920/891	632/392	586/210	572/185	545/161
Thermal conductivity λ/(W/m K)	12.9/15.4	18.2/21.8	20.8/25.4	21.6/26.7	22.9/27.9	24.5/28.8	27.8/29.4
Specific heat °C/g k	0.44/0.44	0.56/0.60	0.60/0.62	0.76/0.66	0.79/0.62	0.79/0.60	0.80/0.61
Poisson ratio μ	0.32/0.31	0.34/0.37	0.36/0.42	0.38/0.39	0.42/0.48	0.45/0.52	0.47/0.46
linear expansive coefficient $\partial/10^{-6}$ °C	12.5/11.2	13.2/11.8	13.6/12.5	14.8/13.7	15.3/14.8	15.7/15.5	15.9/16.9

temperatures. Temperature-dependent material properties are given in Table. 3 based on the experiment test.

In thermal analysis, the reasonable heat source model can improve simulation precision. In this paper, a Gauss distribution heat source model which suits for thin-wall impeller blade was chose. The governing equations are shown in Eqs. (1) and (2) [16]. The diagrammatic drawing is shown in Fig. 4a, and FE model of heat source simulated by ANSYS is shown in Fig. 4b.

$$q(r,z) = \frac{\eta Q e^3}{\pi z_i (e^3-1)\left(r_e^2 + r_e r_i + r_i^2\right)} \exp\left(-\frac{3r^2}{r_0^2}\right) \tag{1}$$

$$r_0(z) = f(z) = r_e - \frac{(z-z_e)}{z_i - z_e}(r_e - r_i) \tag{2}$$

where $q(r,z)$ is heat flux, η is average absorptivity of laser cladding material, Q is heat input power, r is heating radius, and z is heat source longitude.

3.2 Stress-strain relationship

During the laser cladding process, the elastic stress-strain relationship of the material is assumed to obey isotropic Hooke's law. Total strain increment ($\Delta\varepsilon$) can be decomposed into five components, which are elastic ($\Delta\varepsilon_{ij}^e$), plastic ($\Delta\varepsilon_{ij}^p$), thermal loading ($\Delta\varepsilon_{ij}^t$), volumetric change, and transformation plasticity [17]. In order to reasonably reduce the difficulty of convergence in nonlinear thermo-mechanical FE analysis, a thermal-elastic-plastic model was used to study the thermally induced stress evolution and final residual stress in laser cladding process. Therefore, the strain increment can be expressed as:

$$\Delta\varepsilon = \Delta\varepsilon_{ij}^e + \Delta\varepsilon_{ij}^p + \Delta\varepsilon_{ij}^t \tag{3}$$

The elastic and thermal strains can be expressed as:

$$\Delta\varepsilon_{ij}^e = \frac{1+v}{E}\sigma_{ij} - \frac{v}{E}\sigma_{kk}\sigma_{ij} \tag{4}$$

$$\Delta\varepsilon_{ij}^p = \alpha\sigma_{ij}\Delta T \tag{5}$$

Where v is Poisson's ratio, E is Young's modulus, $\alpha$is thermal expansion coefficient and T is temperature. σ_{ij} is defined in following form:

$$\sigma_{ij} = \begin{cases} 1 & \text{for} \quad i = j \\ 0 & \text{for} \quad i \neq j \end{cases} \tag{6}$$

In residual stress analysis, the temperature distribution obtained from thermal analysis was used to calculate the residual stress. And the "birth and death" technology was also used in this section. The material properties related to residual stress are elastic modulus, yield stress, Poisson's ratio, and linear expansive coefficient.

3.3 Boundary and initial conditions

In order to solve energy balance equation, the initial boundary conditions are:

$$\begin{aligned} T(x,y,z,t=0) &= T_o \\ T(x,y,z,t=\infty) &= T_o \end{aligned} \tag{7}$$

The initial ambient temperature (T_0) is set at 20 °C. During the thermal analysis, the heated elements have

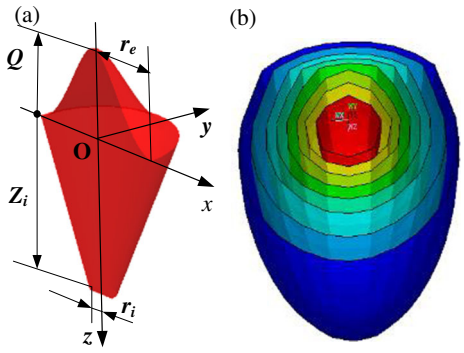

Fig. 4 Heat source model. **a** Diagram of heat source. **b** Finite element model of heat source

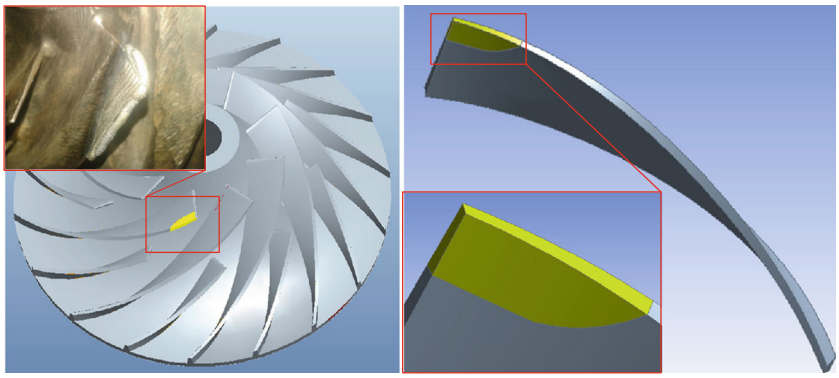

Fig. 5 Geometrical model of remanufactured impeller blade

two main ways including thermal radiation and heat convection to exchange heat to the surroundings. Thus both convection and radiation should be taken into consideration. During stress analysis, nodes of A, B, C, and D at the end of the bottom showed in Fig. 6 were constrained. In this way, rigid body motion could be avoided.

3.4 Finite element model

According to numerical procedure, 3D-remanufactured impeller model was built by software Pro/E (version 5.0) based on 3D surface reverse technology [19]. In order to reduce computing amount, a single remanufactured impeller blade, instead of the whole impeller, was applied to do the laser cladding simulation. The geometrical model is shown in Fig. 5.

In meshing process, a non-uniform mesh was used to improve simulation accuracy and reduce computational cost. Figure 6 shows the FE model for laser cladding, and in total, there are 6622 nodes and 4896 elements meshed. As the blade thickness is 1.1~1.5 mm, which is less than the laser diameter 3 mm, the blade can be directly deposited by a single layer as shown in Fig. 6. Six cladding layers were deposited in total, and the scan path was from left to right along the scaning direction. In transient thermal analysis, thermal conduction element solid70 was used. After completing the thermal analysis, the element type in mechanical analysis was solid187 with quadratic displacement behavior.

4 Remanufactured impeller performance analysis

The failure impeller was remanufactured successfully by laser cladding. Figure 7 shows the remanufactured impeller; the cladding is fine, uniform, and free of crack. In the next section, forming mechanism, microstructure, and remanufactured impeller quality will be discussed in detail.

4.1 Thermal analysis of laser cladding

Figure 8 shows the laser cladding temperature distribution with laser power of 1.1 kW, scanning speed of 5 mm/s, and powder flow rate of 8.0 g/min. Figure 8a shows the isothermal distribution of the temperature contour at 1.2 s. In laser cladding remanufacturing process, the surface of substrate (blade) was heated and melted by laser. At the same time, FeCrNiCu alloy powder was also molten into the substrate to make a cladding layer. The thermal gradient is very important for the mechanical properties of cladding layer. In order to melt the surface of substrate and powder, a large amount of heat was input to a limit area at a very short time, especially in the melt zone. Thus, the melt zone or the near area had very high temperature and a very sharp thermal gradient. This large amount of heat caused residual stress generation and influenced microstructure of cladding. Figure 8b–f shows the key step (t = 0.3, 2.7, 6.6, 9.0, 11.7 s) temperature distribution of laser cladding. The maximum temperature

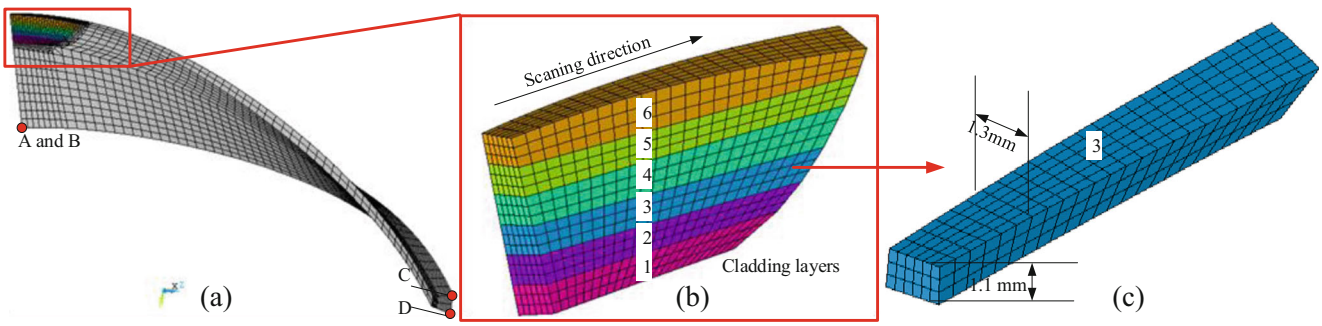

Fig. 6 Mesh model of the remanufactured impeller blade (**a**) Blade mesh (**b**) Laser cladding zone mesh (**c**) The third cladding layer mesh

Fig. 7 Remanufactured impeller

is in the center of laser spot, which can reach to 1521 °C. Along the scanning direction, the molten pool moved forward and continuously cooled. In front of the cladding pool, the isotherms are intensive with high temperature grade. Figure 8b shows temperature in step 1 at 0.3 s, and the max temperature is 1240 °C. As there is no heat accumulation in the first stage, the difference value of temperature between the first step and other steps is about 240 °C. In order to improve the quality of remanufactured impeller, the laser power should be increased to improve the temperature of cladding pool in initial stage.

In laser cladding process, heats will increase continuously during layer by layer forming, which will generate a large thermal stress in the forming layer. The thermal stress directly affected geometric precision of the impeller, and even cracks will occur in cladding layers. Figure 9 shows contours of von Mises equivalent stress distribution in key steps (t = 4.2 s, t = 5.4 s, t = 323.4 s). From the Fig. 9a, higher stress concentration is located at cladding zone and surrounding HAZ and the max stress is 270 MPa. Figure 9b shows the von Mises equivalent stress distribution at 1.2 s, the max stress is 316 MPa, and the stress is mainly concentrated at the interface of layers. Figure 9c shows the stress of blade after cooling. The residual stresses are partially relived and the max

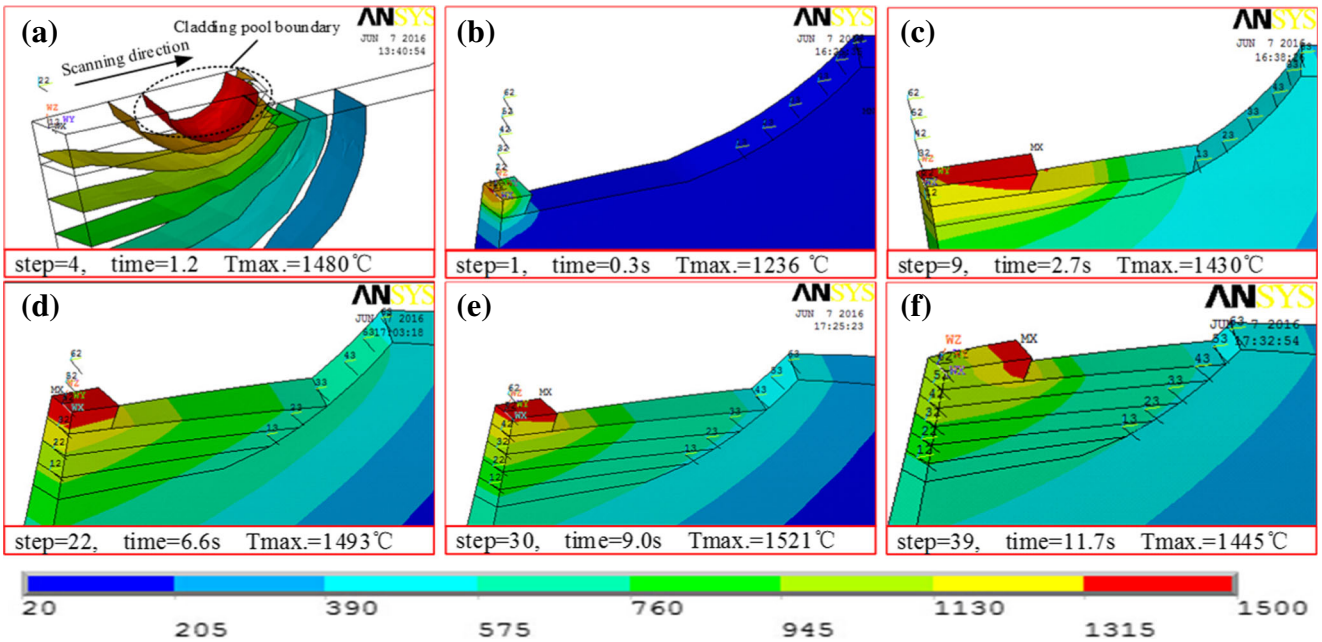

Fig. 8 Temperature distributions in key steps in laser cladding. **a** step = 4, **b** step = 1, **c** step = 9, **d** step = 22, **e** step = 30, and **f** step = 39

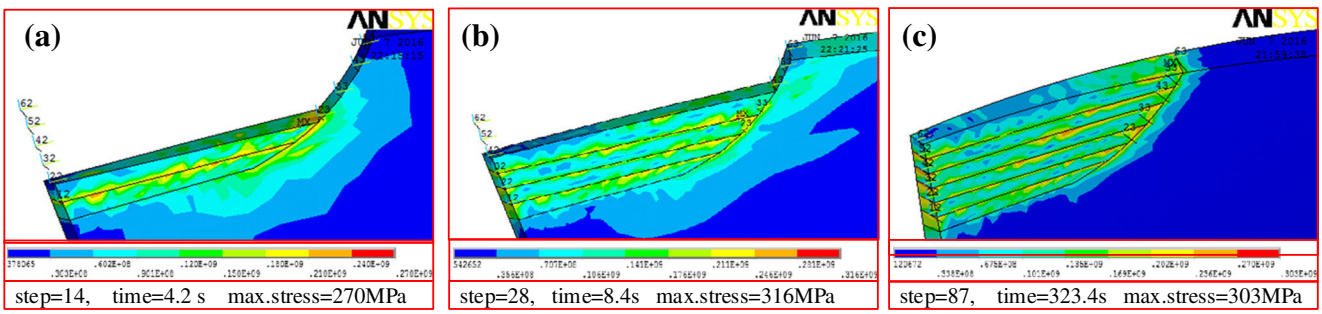

Fig. 9 Von Mises equivalent stress of blade impeller. **a** step = 14, **b** step = 28, and **c** step = 87

Fig. 10 Residual stress measurement by XRD

stress is 303 MPa. It is concluded that the residual stresses are generated after laser cladding in cladding coatings; the max stress is about 300 MPa. In order to validate the simulation model, the residual stress was tested by X-ray diffraction (XRD), as shown in Fig. 10. The experimental results show good consistency with simulation results. A reasonable heat treatment could be conducted to improve the quality of remanufactured impeller by relieving residual stress.

As thermal stress existed in cladding layers, the deformation of blades was generated. The large deformation will cause harmful deflection, which seriously affects stability and safety of the centrifugal compressor. It is hard to obtain high precision deformation by finite element analysis (FEA) due to different laser cladding parameters, various control boundaries, different heat treatment methods, etc. Thus, FEA method was used in strain analysis and Power Scan-IIS 3D scanner was used in deformation analysis. Figure 11 shows the strain and deformation of remanufactured blade. Figure 11a is the strain contour of blade at 323.4 s. As a large amount of heat is input in a limit area at a very short time, the strain is mainly concentrated on the cladding layers. Figure 11b is deformation contour obtained by 3D scanner and deformation is 1.5 mm. The deformation position is in good agreement with simulation results and the simulation model is validated. After laser cladding, the impeller will be machined to meet the requirements of

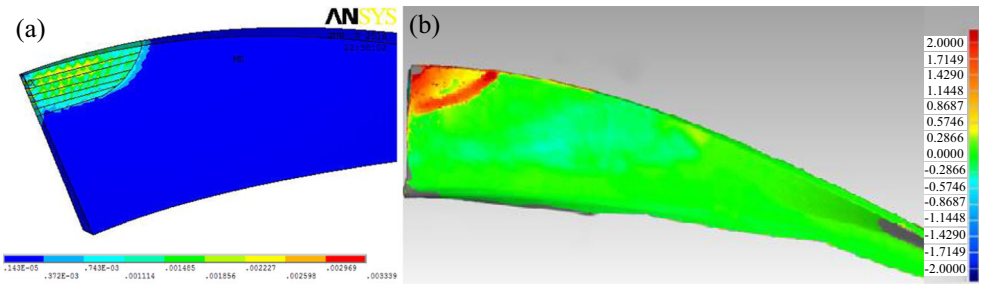

Fig. 11 Strain/deformation of remanufactured blade. **a** Strain of remanufactured blade. **b** Deformation of remanufactured blade

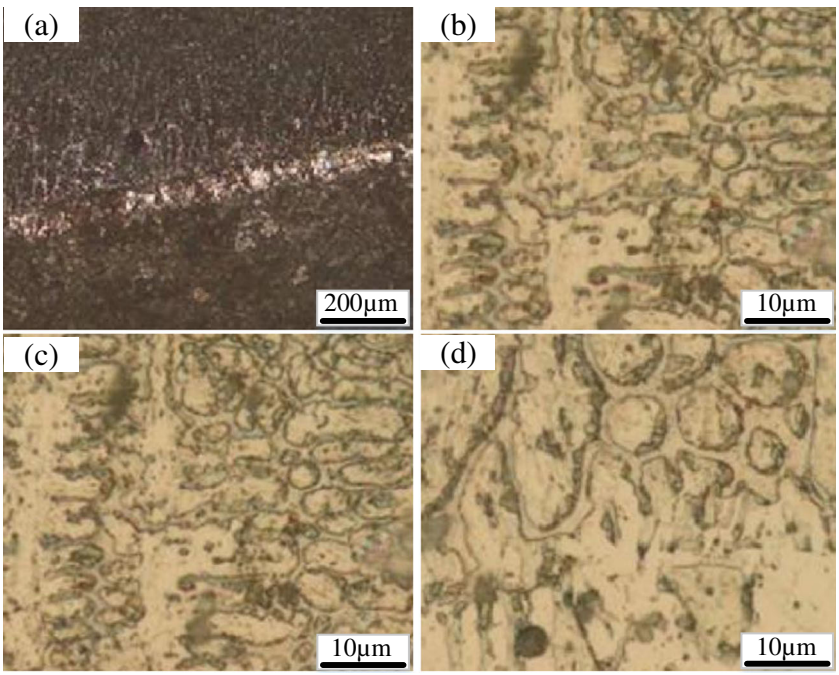

Fig. 12 Microstructure of cladding zone. **a** Interface of cladding and substrate. **b** Top cladding zone. **c** Middle cladding zone. **d** Bottom cladding zone

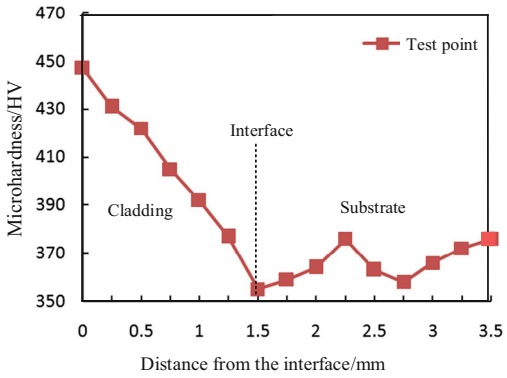

Fig. 13 Microhardness of cladding and substrate

impeller and the deformation of 1.5 mm can be eliminated through machining process.

4.2 Microstructure of cladding zone

4.2.1 Microstructure

The performance of joint between cladding and substrate is closely related to the quality of remanufacturing impeller. In this paper, metallurgical bonding interface and cladding layer were observed by metallurgical microscopy as shown in Fig. 12. From the Fig. 12a, intermittent white bright band can be easily observed in the bonding interface, with a thickness of about 30 μm. White bright band is mainly composed of a plane crystal structure, which is determined by heat transfer between the substrate and cladding layer. Based on the properties of FeCrNiCu alloy, the strengthening phase of M_7C_3 and NbC carbide dispersed in the Fe based alloy can improve bonding strength and microhardness of the forming part. From Fig. 12b, the top of cladding layer consists of fine equiaxed grains, and a large number of strengthening phases are precipitated in grain and grain boundaries. Due to the negative temperature gradient generation which caused by sharp thermal diffusivity, a large number of fine crystalline particles are formed. From Fig. 12c, the middle of cladding layer mainly consists of dendrite. In the dendrite, the secondary phase separation is precipitated which can improve the high microhardness under the dispersing strengthened effect. The ferrite and Cr_7C_3 are found in the laser

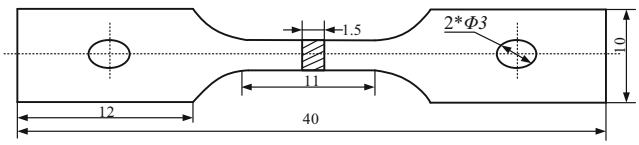

Fig. 14 Tensile specimen

Table 4 Tensile strength of experiment

	Test/MPa	Average/MPa
Laser cladding specimen	961	873
	845	
	812	
FV520B specimen	1020	1091
	1175	
	1078	

cladding coating by XRD phase analysis. These strengthening phases can improve mechanical properties due to high microhardness, high bonding strength, good wear resistance, and strong corrosion resistance. Figure 12d shows the microstructure of the bottom of cladding layer. The fine grained austenite and undissolved carbides particles are existed in grain and grain boundaries. The cladding layer and the substrate have a good metallurgical bonding, which ensures high bonding strength of the cladding layer.

4.2.2 Microhardness

The microhardness of cladding cross section was tested by DSZF-1 digital microhardness tester. In the thickness direction of a cladding layer, 15 points were selected. The microhardness of every point was calculated by taking the average of the remaining 4 points in horizontal line apart 0.3 mm. The microhardness is shown in Fig. 13. The surface microhardness of the cladding layer is the highest, and the average value is 443 HV. As a lot of strengthening phases (M_7C_3, NbC) decarbonized in the cladding layer, the microhardness is increased. From the top to the interface, the microhardness decreased gradually, and the hardness decreased to 361 HV. As the crystal microhardness is transformed from the equiaxial grains to the dendrite, the microhardness is decreased slightly. The average value of cladding layer

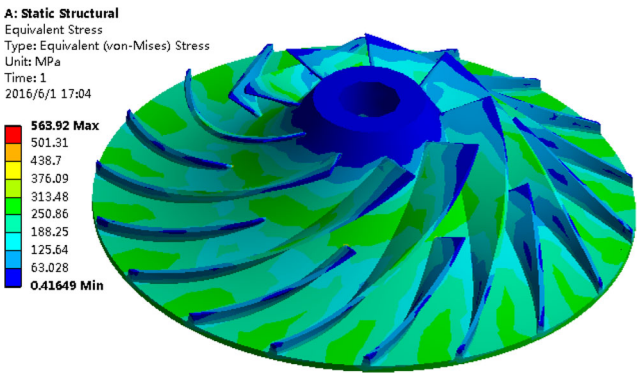

Fig. 15 Von Mises equivalent stress at rated speed

Fig. 16 Dynamic balance test

is 398 HV. From the interface to substrate, the microhardness increased gradually and remained relatively stable; the average microhardness is 360 HV. The substrate was diluted with cladding layer in laser cladding, and the microhardness is remained stable.

4.2.3 Tensile property

In order to study the bonding strength between cladding layer and substrate, the tensile test was carried out by using INTRON 9 tensile testing machine. The loading rate was $v = 0.02$ mm/s, and tensile load was $\sigma = 0.003$ kN. The tensile specimen is shown in Fig. 14. The results were recorded by a computer.

Table 4 is the result of tensile testing. The results show that the max tensile strength of FeCrNiCu-FV520B specimen is 961 MPa and the tensile strength range is 812~961 MPa. The tensile strength of FV520B specimen is 1020~1178 MPa. The tensile strength of the laser cladding specimen is lower than that of specimen FV520B, but it still has a very high tensile strength.

4.3 Remanufactured impeller quality test

Impeller is easy to fail under combined action of centrifugal force, aerodynamic stress, and wake excitation [20]. Figure 15 shows the equivalent stress of impeller at the rated speed by FEA. The equivalent stress of the impeller is as high as 563.92 MPa. So, it is necessary to assess the safety of remanufactured impeller.

The safety testing method of impeller mainly includes dynamic balance test, over-speed test, crack test, and nondestructive test (NDT). As the rotational speed of impeller was very high, a small amount of unbalance quantity can cause accident at rated speed. Figure 16 shows the dynamic balance test experiment. The two-planes of remanufactured impeller were tested to ensure that the impeller is in a standard equilibrium state. The unbalance quantity can be calculated by the Eq. (8).

$$m = M \times G \times \frac{60}{2\pi \times r \times n} \times 10^3 \tag{8}$$

Where m is the unbalance quantity (g), M is weight of remanufactured impeller (kg), G is balance accuracy level of the impeller (mm/s), r is radius of impeller (mm), and n is rotational speed (rpm).

According to the test, m is less than 0.3 g which meets the requirements of impeller. As the composition of FeCrNiCu is similar to that of FV520B, there is no difference in density. Meanwhile, the high-precision machining method was adopted after laser cladding. Thus, the m is very small.

The safety of remanufactured impeller under bad conditions also should be considered. The over-speed test of impeller can not only test the safety at high speed but also release part of residual stress to enhance safety. Figure 17a shows the over-speed test experiment. By using this experiment, the manufactured impeller was tested 3 min at 115 % rated speed. In order to test the impeller quality after over-speed test, the dye penetration inspection technique (DPIT) was adopted to detect the cracks invisible to the naked eyes of the remanufactured impeller. The result is shown in Fig. 17b after cleaning the remanufactured impeller with the cleaning agent. In over-speed test, no abnormal phenomenon occurred. Further dye penetration inspection shows that there are no cracks on the surface of remanufactured impeller.

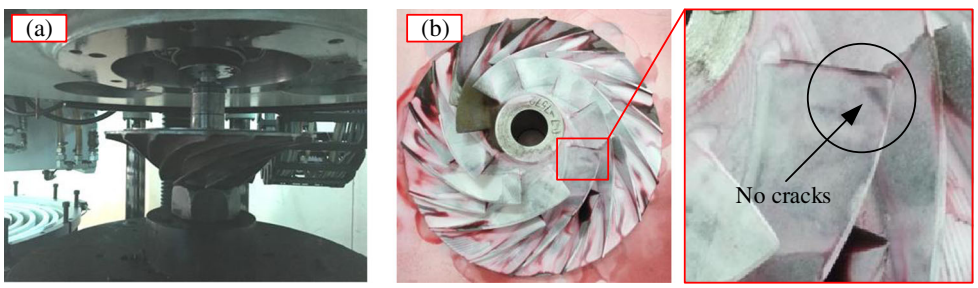

Fig. 17 Remanufactured impeller safety test. **a** Over-speed test. **b** Dye penetration inspection

5 Conclusions

The centrifugal compressor impeller is widely used in petroleum, chemicals, military, and other important fields. In this paper, the laser cladding remanufacturing process with FeCrNiCu alloy powder for thin-wall impeller blade was studied. Based on present study, several points can be concluded as follows:

(1) Thermal mechanism of laser cladding was analyzed by FEA. In the initial stage of laser cladding, the temperature was about 1200 °C which was lower than the temperature (1521 °C) in a steady state of cladding pool. The laser power should be increased in the initial stage. Residual stress analysis showed that the generated equivalent stress was about 310 MPa in HAZ. Therefore, it is necessary to reduce residual stress of remanufactured impeller by reasonable heat treatment. The deformation of remanufactured impeller was 1.5 mm.
(2) The cladding layers were analyzed by metallurgical microstructure, microhardness, and tensile property test. The metallographic structure of cladding coatings was compact and continuous without cracks and pores. The strengthening phases of ferrite and Cr_7C_3 can improve the mechanical properties. The average microhardness of cladding was 361 HV, and the tensile strength was about 860 MPa.
(3) The safety tests were carried out by dynamic balance test, over-speed test, and DPIT. The unbalance quantity of m was less than 0.3 g, and no cracks occurred in DPIT analysis after over-speed test at 115 % rated speed.

As the quality and safety of remanufactured impeller are related to failure modes, work conditions, powders, laser cladding processing parameters, etc., the fatigue life will be different. Thus, the study about fatigue life assessment will be performed in the next study.

Acknowledgments The authors are thankful for the financial support provided by the National Basic Research Program of China (project number: No.2011CB013405). Also, the authors thank for the experiment support from Professor Haidou Wang et al. in the Academy of Armored Forces Engineering, China.

References

1. Sonthipermpoon K, Bohez E, Hasemann H, Rautenberg M (2010) The vibration behavior of impeller blades in the five-axis CNC flank milling process. Int J Adv Manuf Technol 46(9):1171–1177
2. Wilson JM, Piya C, Shin YC, Zhao F, Ramani K (2014) Remanufacturing of turbine blades by laser direct deposition with its energy and environmental impact analysis. J Clean Prod 80(80): 170–178
3. Egusquiza E, Valero C, Presas A, Huang X, Guardo A, Seidel U (2015) Analysis of the dynamic response of pump-turbine impellers influence of the rotor. Mechanical Systems & Signal Processing 68-69:330–341
4. Zhang M, Liu Y, Wang W, Wang P, Li J (2016) The fatigue of impellers and blades. Eng Fail Anal 62:208–231
5. Zhang P, Liu Z (2015) Machinability investigations on turning of Cr-Ni-based stainless steel cladding formed by laser cladding process. Int J Adv Manuf Technol 82:1707–1714
6. Dong SY, Yan SX, BS X, Wang YJ, Ren WB (2013) Laser cladding remanufacturing technology of cast iron cylinder head and its quality evaluation. Journal of academy of armored force. Engineering 27(1):90–93
7. Hu YH, Tian YJ, Chen CN, Ruan ZJ, Zhang Z, Zhong QP, Hang BC (2008) Failure analysis on laser cladding repaired GH864 alloy rotating blades of flue gas turbines. Heat Treatment of Metals 5:96–99
8. Rottwinkel B, Nölke C, Kaierle S, Wesling V (2014) Crack repair of single crystal turbine blades using laser cladding technology. Procedia Cirp 22(1):263–267
9. Lin CM (2015) Parameter optimization of laser cladding process and resulting microstructure for the repair of tenon on steam turbine blade. Vacuum 115:117–123
10. Chew YX, Pang JHL, Bi GJ, Song B (2015) Thermo-mechanical model for simulating laser cladding induced residual stresses with single and multiple clad beads. J Mater Process Technol 224:89–101
11. Jiang WC, Liu Z, Gong JM, Tu ST (2010) Numerical simulation to study the effect of repair width on residual stresses of a stainless steel clad plate. International Journal of Pressure Vessels & Piping 87(8):457–463
12. Jia WP, Lin X, Tan H, Yang HO, Zhong CW, Huang WD (2007) Numerical simulation for temperature field of TC4 titanium alloy hollow blade during laser rapid forming process. Rare Metal Mater Eng 36(7):1193–1199
13. Thiago FA, Raphael CC, Paulo RTS, Abraão SS, Sandro G (2016) Analysis of turbo impeller rotor failure. Eng Fail Anal 63:12–20
14. Chu QL, Zhang M, Li JH (2013) Failure analysis of impeller made of FV520B martensitic precipitated hardening stainless steel. Eng Fail Anal 34(1):501–510
15. Zhang M, Wang WQ, Wang PF, Yan LIU, Li JF (2014) Fatigue behavior and mechanism of FV520B-I in ultrahigh cycle regime. Procedia. Mater Sci 3:2035–2041
16. Al-Khairy RT (2011) Thermal wave propagation in a finite medium irradiated by a heat source with Gaussian distribution in both the temporal and spatial domain. Int J Therm Sci 50(8):1369–1373
17. Kong F, Ma J, Kovacevic R (2011) Numerical and experimental study of thermally induced residual stress in the hybrid laser–GMA welding process. J Mater Process Technol 211(6):1102–1111
18. Farahmand P, Kovacevic R (2014) An experimental–numerical investigation of heat distribution and stress field in single- and multi-track laser cladding by a high-power direct diode laser. Optics & Laser Technology 63(4):154–168
19. Xu L, Cao HJ, Shu LS (2016) 3-D modeling and hexahedral mesh generation method based on failure characteristics of remanufactured centrifugal compressor impeller. Journal of Industrial and Production Engineering 33(5):339–347
20. Liu SJ, Liu C, YW H, Gao SB, Wang YF, Zhang HC (2016) Fatigue life assessment of centrifugal compressor impeller based on FEA. Eng Fail Anal 60:383–390